Binding-Promoted Chemical Reaction in the Nanospace of a Binding Site: Effects of Environmental Constriction

Journal:	*Organic & Biomolecular Chemistry*
Manuscript ID	OB-COM-03-2018-000590.R1
Article Type:	Communication
Date Submitted by the Author:	30-Mar-2018
Complete List of Authors:	Xing, Xiaoyu; Iowa State University, Department of Chemistry Zhao, Yan; Iowa State University, Department of Chemistry

Journal Name

COMMUNICATION

Binding-Promoted Chemical Reaction in the Nanospace of a Binding Site: Effects of Environmental Constriction

Xiaoyu Xing and Yan Zhao*[a]

Received 00th January 20xx,
Accepted 00th January 20xx

DOI: 10.1039/x0xx00000x

www.rsc.org/

Chemical reactions in a confined nanospace can be very different from those in solution. Imine formation between molecular amines and an aldehyde inside a molecularly imprinted receptor was promoted strongly by the binding. Although how well the amine fit in the binding pocket and its electronic nature both influenced the reaction, the freedom of movement for the amine was the most important factor determining the binding-normalized reactivity.

Molecules often behave very differently in confined nanospace than in a homogeneous solution. The steric constriction imposed on them sometimes gives rise to unusual chemical reactivity and selectivity.[1, 2] Diel–Alder reaction, for example, can occur at the 1,4- instead of the normal 9,10-positions of anthracene.[3, 4] Regio- and stereoselectivity of chemical reactions sometimes are dramatically altered within self-assembled capsules.[5-8]

Molecular imprinting[9, 10] is a powerful technique to create guest-complementary binding sites useful for many applications.[11-22] We recently prepared a novel class of molecularly imprinted nanoparticles (MINPs) through templated polymerization in cross-linkable micelles.[23-26] Our method also allowed us to install a single carboxylic acid group inside the binding site using a photocleavable template. Because MINPs are soluble in water and selected organic solvents such as DMF, we could perform chemical reactions (amide formation) inside the MINP binding pocket to modulate their binding properties.[25]

Postfunctionalization of imprinted binding sites is extremely important to their molecular recognition.[27-31] Although the above photocleavage and postfunctionalization worked well, it was difficult to obtain further insight into the reaction that occurred in the nanospace of the MINP binding site. Synthesis of the photocleavable templates was also quite cumbersome.

In this work, we employed an imine-based template–functional monomer (T–FM) complex to introduce an aldehyde group inside the MINP binding site. Not only was the synthesis more straightforward, the fluorescent amine used also enabled us to study the binding-promoted chemical reaction by fluorescence spectroscopy.

As shown by Scheme 1, synthesis of MINPs involved three simple steps: surface-cross-linking of the micelle by click reaction, surface-decoration by click reaction, and core-cross-linking by UV-initiated free radical polymerization (details are reported in the ESI).[23-26] They were characterized by ^{1}H NMR spectroscopy, dynamic light scattering (DLS), and binding studies (vide infra). The DLS size has been confirmed by transmission electron microscopy.[32, 33]

There are several considerations in the design of the T–FM complex **4**. First, imine is formed readily from the corresponding aldehyde and amine, especially with aromatic amines.[34] Second, although imine is quite stable in many solvents, its hydrolysis is easily accomplished in acidic water, meanwhile creating a template-shaped binding site with an aldehyde group at the predetermined position. The covalent imprinting utilized has the benefit of particularly high structural fidelity. Third, amine **5** and its analogues (**6**–**9**) are all fluorescent, allowing us to monitor by fluorescence spectroscopy both the acid-catalyzed hydrolysis (to vacate the binding site) and the re-formation of the imine in the MINP binding pocket.

We used 6 M aqueous HCl solution at 95 °C to hydrolyze the imine of MINP$_4$—i.e., MINP prepared with T-FM complex **4**. The naphthyl group emitted at 405 nm in the MINP. Upon hydrolysis, the fluorescent peak decreased gradually and retained ca 10% of the initial intensity after 300 min (Fig. S7 in ESI). Since the naphthyl group was the only good fluorophore in MINP$_4$, the result was interpreted as successful hydrolysis and removal of the majority of amine **5**. Meanwhile, DLS showed unchanged particle size (~5.5 nm, Fig. S8), suggesting that the acid did not cause decomposition of the rest of the nanoparticle.

[a] *Department of Chemistry, Iowa State University, Ames, Iowa 50011-3111, USA. Fax: + 1-515-294-0105; Tel: +1-515-294-5845; E-mail: zhaoy@iastate.edu.*
Electronic Supplementary Information (ESI) available: Experimental details, fluorescence titration curves, and additional figures. See DOI: 10.1039/x0xx00000x

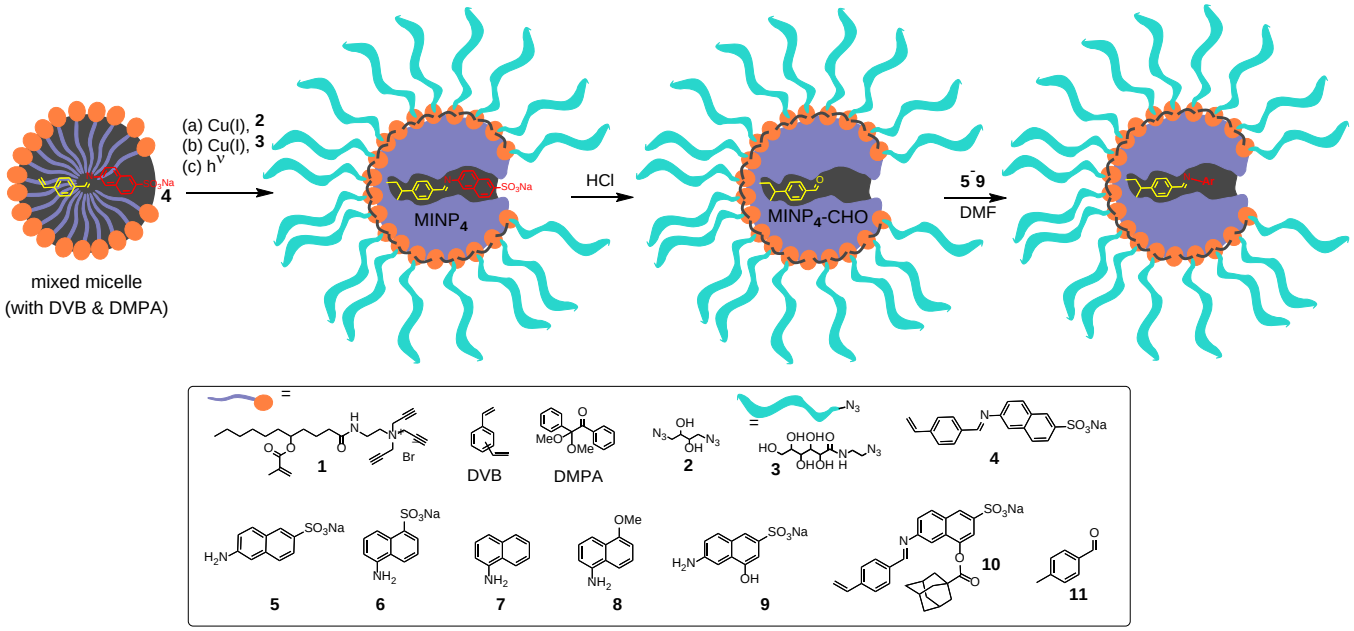

Scheme 1. Preparation of MINP$_4$-CHO by micellar imprinting and hydrolysis, followed by imine formation with **5**–**9**.

Further confirmation of the hydrolysis came from the binding study. Once the imine was hydrolyzed, MINP$_4$-CHO should have a binding pocket tailored precisely for amine **5**. Because the imine formation occurred in DMF (vide infra), we performed the binding study first in DMF.

Fig. 1a shows the fluorescence spectra of **5** upon addition of different concentrations of MINP$_4$-CHO (i.e., the acid-hydrolyzed MINP$_4$). The titration partially quenched the naphthyl emission and afforded two isoemissive points, indicating a continuous transition from the free to the bound template. The fluorescence data fit well to a 1:1 binding isotherm, yielding a binding constant of K_a = (62 ± 5) × 10^4 M^{-1} (Fig. 1b; Table 1, entry 1).

The binding stoichiometry was verified by the Job plot, which showed a clear maximum at 0.5 molar fraction (Fig. S9).

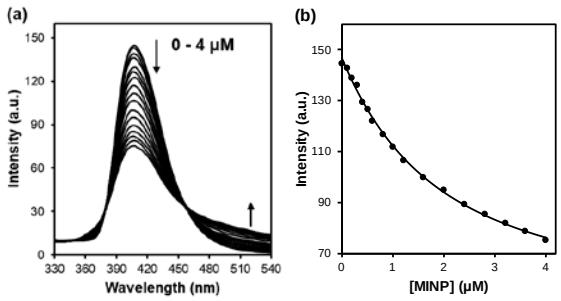

Fig 1. (a) Emission spectra of **5** upon the addition of 0–4 μM MINP$_4$-CHO in DMF at room temperature. [**5**] = 0.5 μM. λ_{ex} = 295 nm. The concentration of the MINP was calculated based on a M.W. of 50000 g/mol determined by DLS. (b) Intensity of **5** at 406 nm as a function of [MINP$_4$-CHO]. The smooth curve was the nonlinear least squares curve fitting of the emission intensity to a 1:1 binding isotherm.

Thus, the MINP receptor had on average one binding site per nanoparticle. Our MINP is estimated to contain ~50 cross-linkable surfactants per nanoparticle by light scattering.[23] We normally keep the surfactant/template ratio at 50:1. The single binding site on MINP$_4$-CHO is consistent with the stoichiometry and a high yielding cleavage reaction.

Table 1 lists the binding constants obtained in this study. Compounds **5** and **6** differ in the substitution pattern on the naphthyl ring. As shown by the K_a values in the parentheses, MINP$_4$-CHO bound **5** (its own template) more strongly than **6** in HEPES buffer. This was an expected result from molecular imprinting and consistent with many studies we have done using micellar imprinting.[23-26, 35-37]

In DMF, however, the opposite became true, with **6** bound much more strongly than **5**. It is not exactly clear why there was

Table 1. Binding data for MINP-CHO and MINP-CH$_2$OH.[a]

Entry	Host	Guest	K_a in DMF (× 10^4 M^{-1})
1	MINP$_4$-CHO	**5**	62 ± 5 (200 ± 30)
2	MINP$_4$-CHO	**6**	1300 ± 800 (73 ± 1)
3	MINP$_4$-CHO	**7**	62 ± 18
4	MINP$_4$-CHO	**8**	43 ± 8
5	MINP$_4$-CHO	**9**	430 ± 120
6	MINP$_4$-CH$_2$OH	**5**	50 ± 8
7	MINP$_{10}$-CHO	**5**	8.8 ± 0.8
8	MINP$_{10}$-CHO	**6**	25 ± 11
9	MINP$_{10}$-CHO	**9**	23 ± 2

[a] The titrations were performed in duplicates and the numbers given were averages of the two runs. The binding constants in parentheses were for titrations performed in 10 mM HEPES buffer (pH 7). The titration curves are found in the ESI (Fig. S10–S20).

such a reversal but the result suggests that hydrophobic interactions in water were essential for the excellent selectivity observed in our previous MINP bindings.[23-26, 35-37] Formation of micelles and the interactions between the template and the micelle in water both have strong hydrophobic contributions. Hydrophobic interactions, however, are eliminated in DMF. Other interactions such as electrostatics (vide infra) might become more important. Not only so, the organic solvent is expected to penetrate into the cross-linked micelle to cause it to swell. A change of the binding pocket could occur as a result.

The binding studies in DMF showed that electrostatic interactions played an important role, as removal of the sulfonate (in **7**) and substitution of the sulfonate with a methoxy (in **8**) weakened the binding of **6** dramatically. Since MINP$_4$-CH_2OH, obtained by treating MINP$_4$-CHO with a large amount of $NaBH_4$, was used as a control to study the imine formation (vide infra), we also studied the binding of **5** by MINP$_4$-CH_2OH. As expected, the two binding constants were fairly similar (Table 1, entries 1 and 6), suggesting that an aldehyde or hydroxyl group inside the binding site did not affect the interactions with the amine template significantly.

MINP$_{10}$-CHO was prepared similarly using template–FM complex **10**. After removal of the template, MINP$_{10}$-CHO should have a large adamantane-shaped pocket near the binding site for the naphthyl group. We designed this template to investigate how freedom of movement for the amine in the binding pocket might influence the imine formation. As far as the binding was concerned, all the sulfonated naphthyl amines could still be bound by this MINP but the binding constants generally decreased—a reasonable result for a less perfectly fitted binding pocket (Table 1, entries 7–9).

We then studied the reactions between various amines (**5**–**9**) and the aldehyde inside the MINP binding site (Table 2). Because the reaction was too slow at 25 °C, we performed the majority of the reactions at 50°C.[38] Two control experiments were also performed using molecular aldehyde **11** (entry 8) and MINP$_4$-CHOH (entry 9), respectively, in the reaction.

For the imine formation, we mixed 0.5 μM **5** and 10 equiv MINP$_4$-CHO in DMF so that the change of concentration for MINP$_4$-CHO was minimal during the reaction (i.e., under pseudo first order kinetics). At room temperature, the fluorescence spectrum of the mixture changed gradually (Fig. S21) but, at higher temperatures (50 °C), the change was much faster (Fig. S22 and 2a). For the negative controls, the emission were practially unchanged over time (Fig. S27 and S28). In our hands, amine **4** emitted at 407 nm and imine **5** emitted more weakly, at 396 nm (Fig. S32). Since similar weakening and a red shift also occurred in Fig. 2a, we attributed the change to the imine formation. Indeed, the decrease in fluorescence intensity fit well to the pseudo first order kinetics and all the rate constants are given in Table 2.

Binding clearly promoted the imine formation, in a dramatic way. Fig. 2b shows that the fluorescence of **5** displayed no change under the same condition in the presence of molecular aldehyde **11** (○). Hence, without the help from the binding, imine could not form at all under our experimental conditions.

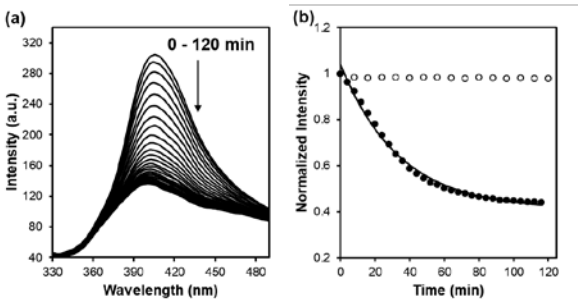

Fig 2. (a) Fluorescence spectra of **5** in the presence of 10 equiv MINP$_4$-CHO in DMF at 50 °C over time. [**5**] = 0.5 μM. λ_{ex} = 295 nm. (b) Emission intensity of **5** in the presence of 10 equiv MINP$_4$-CHO (●) and 10 equiv **11** (○), respectively. The solid line was from fitting of the data to the first-order kinetics.

Table 2. Kinetic data for the imine formation with MINP-CHO.[a]

Entry	Host	Guest	Temp (°C)	k_{obs} in DMF ($\times 10^{-3}$ s^{-1})	k_{obs}/K_a ($\times 10^{-9}$ M·s^{-1})
1	MINP$_4$-CHO	**5**	25	--[b]	--[d]
2	MINP$_4$-CHO	**5**	33	0.032 ± 0.002	--[d]
3	MINP$_4$-CHO	**5**	50	0.49 ± 0.02	0.8
4	MINP$_4$-CHO	**6**	50	0.85 ± 0.10	0.1
5	MINP$_4$-CHO	**7**	50	0.61 ± 0.01	1.0
6	MINP$_4$-CHO	**8**	50	0.75 ± 0.02	1.7
7	MINP$_4$-CHO	**9**	50	1.13 ± 0.06	0.3
8	**11**	**5**	50	--[c]	--[c]
9	MINP$_4$-CH_2OH	**5**	50	--[c]	--[c]
10	MINP$_{10}$-CHO	**5**	50	1.2 ± 0.1	14
11	MINP$_{10}$-CHO	**6**	50	1.1 ± 0.1	4
12	MINP$_{10}$-CHO	**9**	50	1.7 ± 0.2	7

[a] The reactions were performed in duplicates and the numbers given were averages of the two runs.. The fluorescence spectra and the curve fittings are found in the ESI (Figures S21–S31). [b] The reaction was very slow to be measured accurately. [c] No significant change in fluorescence was observed over time.

From the kinetic data in Table 2, the most surprising finding initially was the *insensitivity* of the reaction rates. Although the reaction did become faster at higher temperatures (entries 1–3), the other observed rate constants (k_{obs}) were quite similar, practically within 4–5-fold. Since binding clearly was key to the enhanced reactivity of the aldehyde inside the MINP binding site, we listed the k_{obs}/K_a values for these reactions in Table 2 as well.

The k_{obs}/K_a value could be considered as the binding-normalized rate constant. Once the binding factor was removed, the "intrinsic reactivity" in the nanospace made much sense. For example, as the amine became electron-richer (from **6** to **7** to **8**) while their overall shape stayed very similar, the k_{obs}/K_a value showed a steady increase, from 0.1 to 1 and then to 1.7 × 10^{-9} M·s^{-1} (entries 4–6). This was the expected behavior from the stronger nucleophilicity of the amine. The k_{obs}/K_a value of **5** (entry 3) was 8 times as large as that of **6** (entry 4), indicating that, once the influence of the binding affinity was

removed, the intrinsic reactivity of the original template was still higher than that of the structural analogue. As for compound **9**, its k_{obs}/K_a value was 0.3×10^{-9} M·s^{-1} (entry 7), lower than the 0.8×10^{-9} M·s^{-1} for **5** (entry 3). It is possible that this resulted from a tradeoff between the negative effect of a less perfectly fitted shape and the positive effect of an electron-donating hydroxyl group.

The largest enhancement of the binding-normalized reactivity was observed for MINP$_{10}$-CHO, with k_{obs}/K_a 1–2 orders of magnitude higher than those for MINP$_4$-CHO. Thus, the steric effect seemed to have dominated over the "fitness" of the template and any electronic effects. We attributed this large increase in k_{obs}/K_a to the increased freedom of the amines to move inside the larger binding pocket of MINP$_{10}$-CHO. In order for the imine to form, the amine and the aldehyde groups need to approach each other in preferred angles. Whereas the optimal attacking geometry can be easily achieved in solution by random molecular collision, it could become quite challenging in a constricted nanospace. It is very possible that higher freedom of movement under such a circumstance could be far more important than other factors that tend to dominate in solution chemistry.

In summary, strong binding by MINP not only dramatically enhanced the reaction between a bound amine substrate and the aldehyde in the binding pocket (Figure 2b), the factors that influenced the reaction also became very different, with freedom of movement being the dominant factor in the confined nanospace. Electronic effects, normally a dominant factor in solution chemistry, became secondary in the binding-promoted reactions. We do not think our finding is limited to a particular reaction inside the MINP binding pocket. Similar situations could occur inside a nanopore or within an enzyme active site, wherever movements of molecules are restricted.

We thank NSF (CHE-1708526) for supporting this research.

Notes and references

1. J.-L. Hou, D. Ajami and J. Rebek, *J. Am. Chem. Soc.*, 2008, **130**, 7810-7811.
2. D. M. Kaphan, F. D. Toste, R. G. Bergman and K. N. Raymond, *J. Am. Chem. Soc.*, 2015, **137**, 9202-9205.
3. M. Yoshizawa, M. Tamura and M. Fujita, *Science*, 2006, **312**, 251-254.
4. Y. Nishioka, T. Yamaguchi, M. Yoshizawa and M. Fujita, *J. Am. Chem. Soc.*, 2007, **129**, 7000-7001.
5. L. S. Kaanumalle and V. Ramamurthy, *Chem. Commun.*, 2007, 1062-1064.
6. Z. R. Laughrey, C. L. D. Gibb, T. Senechal and B. C. Gibb, *Chem.-Eur. J.*, 2003, **9**, 130-139.
7. A. Parthasarathy, L. S. Kaanumalle and V. Ramamurthy, *Org. Lett.*, 2007, **9**, 5059-5062.
8. A. Natarajan, L. S. Kaanumalle, S. Jockusch, C. L. D. Gibb, B. C. Gibb, N. J. Turro and V. Ramamurthy, *J. Am. Chem. Soc.*, 2007, **129**, 4132-4133.
9. G. Wulff, *Chem. Rev.*, 2001, **102**, 1-28.
10. K. Haupt and K. Mosbach, *Chem. Rev.*, 2000, **100**, 2495-2504.
11. D. Lakshmi, A. Bossi, M. J. Whitcombe, I. Chianella, S. A. Fowler, S. Subrahmanyam, E. V. Piletska and S. A. Piletsky, *Anal. Chem.*, 2009, **81**, 3576-3584.
12. Y. Hao, R. Gao, L. Shi, D. Liu, Y. Tang and Z. Guo, *J. Chromatogr. A*, 2015, **1396**, 7-16.
13. T. Kuwata, A. Uchida, E. Takano, Y. Kitayama and T. Takeuchi, *Anal. Chem.*, 2015, **87**, 11784-11791.
14. J. Liu, D. Yin, S. Wang, H. Y. Chen and Z. Liu, *Angew. Chem. Int. Ed.*, 2016, **55**, 13215-13218.
15. L. Chen, X. Wang, W. Lu, X. Wu and J. Li, *Chem. Soc. Rev.*, 2016, **45**, 2137-2211.
16. R. Horikawa, H. Sunayama, Y. Kitayama, E. Takano and T. Takeuchi, *Angew. Chem. Int. Ed.*, 2016, **55**, 13023-13027.
17. M. Panagiotopoulou, Y. Salinas, S. Beyazit, S. Kunath, L. Duma, E. Prost, A. G. Mayes, M. Resmini, B. T. S. Bui and K. Haupt, *Angew. Chem. Int. Ed.*, 2016, **55**, 8244-8248.
18. D. Yin, X. Li, Y. Ma and Z. Liu, *Chem. Commun.*, 2017, **53**, 6716-6719.
19. P. K. Paul, A. Treetong and R. Suedee, *Acta Pharm.*, 2017, **67**, 149-168.
20. M. Bertolla, L. Cenci, A. Anesi, E. Ambrosi, F. Tagliaro, L. Vanzetti, G. Guella and A. M. Bossi, *ACS Appl. Mater. Interfaces*, 2017, **9**, 6908-6915.
21. A. Cecchini, V. Raffa, F. Canfarotta, G. Signore, S. Piletsky, M. P. MacDonald and A. Cuschieri, *Nano Lett.*, 2017, **17**, 2307-2312.
22. L. Jiang, M. E. Messing and L. Ye, *ACS Appl. Mater. Interfaces*, 2017, **9**, 8985-8995.
23. J. K. Awino and Y. Zhao, *J. Am. Chem. Soc.*, 2013, **135**, 12552-12555.
24. J. K. Awino and Y. Zhao, *Chem. Commun.*, 2014, **50**, 5752-5755.
25. J. K. Awino and Y. Zhao, *Chem.-Eur. J.*, 2015, **21**, 655-661.
26. J. K. Awino and Y. Zhao, *ACS Biomater. Sci. Eng.*, 2015, **1**, 425-430.
27. N. Kirsch, C. Alexander, M. Lübke, M. J. Whitcombe and E. N. Vulfson, *Polymer*, 2000, **41**, 5583-5590.
28. S. C. Zimmerman, I. Zharov, M. S. Wendland, N. A. Rakow and K. S. Suslick, *J. Am. Chem. Soc.*, 2003, **125**, 13504-13518.
29. K. Takeda, A. Kuwahara, K. Ohmori and T. Takeuchi, *J. Am. Chem. Soc.*, 2009, **131**, 8833-8838.
30. T. Takeuchi, T. Mori, A. Kuwahara, T. Ohta, A. Oshita, H. Sunayama, Y. Kitayama and T. Ooya, *Angew. Chem. Int. Ed.*, 2014, **53**, 12765-12770.
31. H. Sunayama and T. Takeuchi, *ACS Appl. Mater. Interfaces*, 2014, **6**, 20003-20009.
32. S. Fa and Y. Zhao, *Chem. Mater.*, 2017, **29**, 9284-9291.
33. S. Fa and Y. Zhao, *Chem. -Eur. J.*, 2018, **24**, 150-158.
34. R. W. Layer, *Chem. Rev.*, 1963, **63**, 489-510.
35. J. K. Awino, L. Hu and Y. Zhao, *Org. Lett.*, 2016, **18**, 1650-1653.
36. J. K. Awino, R. W. Gunasekara and Y. Zhao, *J. Am. Chem. Soc.*, 2017, **139**, 2188-2191.
37. J. K. Awino and Y. Zhao, *Org. Biomol. Chem.*, 2017, **15**, 4851-4858.
38. The emission intensity of compound **5** was temperature-dependent, as shown by Fig. S21, S22, and 2a.

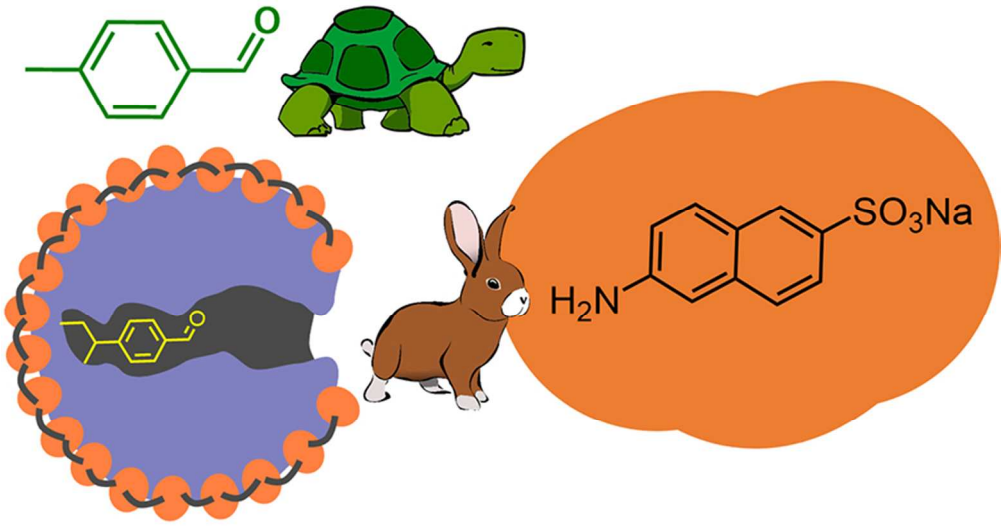

76x39mm (300 x 300 DPI)